Magneto-optical Kerr effect with twisted light beams: the origin of helicoidal dichroism in the reflection off magnetic vortices

Martin Luttmann, Mauro Fanciulli, Matteo Pancaldi, Emanuele Pedersoli, Mekha Vimal, David Bresteau, Maurizio Sacchi, Dario de Angelis, Primoz Rebernik, Benedikt Rösner, et al.

HAL Id: hal-03741786

https://hal-cnrs.archives-ouvertes.fr/hal-03741786

Submitted on 15 Nov 2022

Magneto-optical Kerr effect with twisted light beams: the origin of helicoidal dichroism in the reflection off magnetic vortices

Martin Luttmann [1,2] Mauro Fanciulli [3] Matteo Pancaldi [4] Emanuele Pedersoli [4] Mekha Vimal [1,2] David Bresteau [1,2] Maurizio Sacchi [5,6] Dario de Angelis [4] Primoz Rebernik [4] Benedikt Rösner [7] Carlo Spezzani [4] Ricardo Sousa [8] Ioan-Lucian Prejbeanu [8] Laurent Vila [8] Bernard Dieny [8] Giovanni de Ninno [4,9] Thierry Ruchon [1,2] Flavio Capotondi [4]

[1] LIDyl - Laboratoire Interactions, Dynamiques et Lasers
[2] ATTO Lab - IRAMIS
[3] LPMS - Laboratoire de Physique des Matériaux et des Surfaces
[4] Elettra, Sincrotrone Trieste
[5] INSP - Institut des Nanosciences de Paris
[6] Synchrotron SOLEIL
[7] PSI - Paul Scherrer Institute
[8] SPINTEC - SPINtronique et TEchnologie des Composants
[9] University of Nova Gorica

ABSTRACT

Studying magnetization configurations of ever more complex magnetic structures has become a major challenge in the past decade, especially at ultrashort timescales. Most of current approaches are based on the analysis of polarization and magnetization-dependent reflectivity. We introduced a different concept, centered on the coupling of magnetic structures with light beams carrying orbital angular momentum (OAM), which was recently tested it in an experiment with magnetic vortices. Upon reflection by a magnetic vortex, an incoming beam with a well-defined OAM ℓ gets enriched in the neighboring OAM modes $\ell \pm 1$. It results in anisotropic far-field profiles, which leads to a Magnetic Helicoidal Dichroism (MHD) signal. In this paper we provide a detailed analysis of MHD for the case of a magnetic vortex, providing an intuitive explaination in terms of transverse MOKE. The analysis of MHD allows to retrieve the complex magneto-optical constants. This method, which does not require any polarimetric measurement, is a new promising tool for the identification and analysis of magnetic configurations such as vortices, with a possible extension to the femtosecond to attosecond time resolution.

Keywords: Magneto-optical Kerr effect, magnetic nanostructures, vortex beams, orbital angular momentum, helicoidal dichroism

1. INTRODUCTION

Magnetic nanostructures play a central role in modern technological applications,[1, 2] where prominent examples are data storage,[3] data transfer,[4–6] new computing architectures[7, 8] or biomedical applications.[9, 10] Among a great variety of possible magnetic structures,[11, 12] magnetic vortices (MVs) seem particularly favorable for applications.[13, 14] They appear in mesoscopic circular dots, with a diameter larger than their thickness, and consist of an in-plane magnetic curling and out-of-plane core. Their toroidal moment[15] and polarity, respectively the sense of the magnetic curling and core, allow to describe them as topologically protected quasiparticles that are particularly robust against perturbations.[16] Furthermore, they can be driven out of equilibrium by magnetic fields[17] or spin polarized currents[3] with rich sub-nanosecond dynamics,[18] offering a way to manipulate them.[9, 19]

MVs have been intensely studied using several imaging techniques, such as magnetic force microscopy,[13] Lorentz microscopy[20] or spin-polarized scanning tunneling microscopy.[21] These techniques, while having atomic level spatial resolution, are restricted to slow dynamics; their extension below microsecond resolution remains challenging.[22, 23] Alternatively, at the price of lower spatial resolution, optical methods using ultrashort laser pulses give access to femtosecond dynamics.[24–26] They exploit magneto-optical effects, such as the magneto-optical Kerr effect in reflexion (MOKE), or Magnetic Circular or Linear Dichroism in transmission (MCD, MLD), which are all consequences of light's polarization and surface's magnetization dependence of the complex optical indices. The spatial resolution is limited by the focal spot size, ultimately related to the wavelength of light. Using X-rays, it was possible to combine tens of nanometer spatial resolution with picosecond time resolution using

photoemission electron microscopy[17] or spin-polarized scanning tunneling microscopy combined with MCD and MLD.[27] Furthermore, the analysis of X-rays scattering patterns allows the statistical determination of average magnetic structures of 100 nm size[28] with femtosecond resolution.[29] This latter approach, which considers an incoherent scattering of the incoming light, was also proposed to probe MVs.[30] Conversely, for imaging the exact magnetic structures, the coherence of high harmonic generation sources was lately exploited in combination with MCD in a coherent diffraction imaging setup, yielding images with 50 nm resolution.[31] Here, the image retrieval relies on the analysis of the dichroic diffraction patterns for beams of opposite circular polarization, corresponding to modes of opposite Spin Angular Momentum (SAM).

In recent theoretical[32] and experimental[33] work, we investigated a complementary approach exploiting the Orbital Angular Momentum (OAM) of light, which is indexed by an integer $\ell \in Z$, and concluded that spatially inhomogeneous magnetic structures yield a so-called magnetic helicoidal dichroism (MHD). Both MCD and MHD are linked to the magneto-optical constants. However, MHD primarily depends on the symmetry of the magnetic structure through its azimuthal mode content, making it extremely promising to identify structures, including their signs. It can be observed with any polarization of coherent light beams and vanishes for uniform magnetization. MVs, which have a very simple decomposition on the azimuthal modes, are a privileged test case for MHD, yielding very simple expressions and strong signals.

In this article, we provide a simple and intuitive explanation for MHD in the particular case of MVs. First, we recall the basic principles of MOKE interactions of a linearly polarized light beam with magnetic samples presenting a uniform magnetization. We then analyze the mode content of a light beam reflected by a MV, showing a selective population of OAM modes. Finally, we analyse the corresponding far field images, showing the appearance of MHD.

2. MOKE WITH HOMOGENOUS MAGNETIZATION

Beyond the regular Fresnel coefficients r_{pp} and r_{ss} for respectively the P and S-polarized electric fields *, MOKE coupling constants r_0^t and r_{ps}^l, which are complex numbers, are considered. m_l and m_t are the in-plane magnetization components along the longitudinal and transverse directions with respect to the scattering plane, normalized by the saturation magnetization. In order to keep the formalism simple, we do not consider any polar component of the magnetization. The reflectivity matrix writes:[32, 34]

$$R = \begin{pmatrix} r_{pp} + r_{pp} \cdot r_0^t \cdot m_t & r_{ps}^l \cdot m_l \\ -r_{ps}^l \cdot m_l & r_{ss} \end{pmatrix} \tag{1}$$

In this work, we consider a P-polarized incident beam, and a sample with in-plane magnetization. In order to compare the effects of the two magnetization components on the light field, we first consider a gaussian incident beam, whose Jones representation writes $E_i = \begin{pmatrix} 1 \\ 0 \end{pmatrix}$, and a magnetic material with homogeneous longitudinal magnetization (L-MOKE configuration). The reflected field can be expressed as

$$E_r = \begin{pmatrix} r_{pp} & r_{ps}^l \cdot m_l \\ -r_{ps}^l \cdot m_l & r_{ss} \end{pmatrix} \cdot \begin{pmatrix} 1 \\ 0 \end{pmatrix} = \begin{pmatrix} r_{pp} \\ -r_{ps}^l \cdot m_l \end{pmatrix}. \tag{2}$$

As apparent in Eq. 2, the reflected field has P and S components. However, the phase of both components does not depend on the magnetization strength, but is only given by the arguments of the complex coupling constants r_{pp} and r_{ps}^l.

On the other hand, if the magnetization is purely transverse (T-MOKE configuration), the reflected field writes as

$$E_r = \begin{pmatrix} r_{pp}(1 + r_0^t \cdot m_t) & 0 \\ 0 & r_{ss} \end{pmatrix} \cdot \begin{pmatrix} 1 \\ 0 \end{pmatrix} = \begin{pmatrix} r_{pp}(1 + r_0^t \cdot m_t) \\ 0 \end{pmatrix}. \tag{3}$$

---

*Note that in order for the P and S components of the polarization to be defined, the angle of incidence of the light on the sample cannot be zero, thus we are considering off-normal reflections here.

In this case, the electric field after reflection remains P-polarized, but its intensity has been multiplied by $|r_{pp}(1 + r_0^t \cdot m_t)|$, and it has been dephased by $\arg(r_{pp}(1 + r_0^t \cdot m_t))$. We conclude that T-MOKE is able to change the phase of a P-polarized light beam while leaving its polarization unchanged. Since the OAM of light is related to the shape of the beam's wave-fronts (i.e., the spatial phase) it is clear that magnetic samples with proper transverse magnetization geometry will be able to couple with the OAM of light, through T-MOKE.

3. NEAR-FIELD MOKE WITH A MAGNETIC VORTEX

3.1 Simple derivation of the OAM modes redistribution upon reflection

We now consider a magnetic sample with curling in-plane magnetization, and draw an intuitive view of the reflection of a twisted light beam $E_i = \begin{pmatrix} e^{i\ell\varphi} \\ 0 \end{pmatrix}$ (for now, we neglect the intensity profile of the beam) on such sample. The m_l and m_t components now depend on the azimuth φ in the plane of the sample. We have

$$
\begin{aligned}
m_t &= m \cdot m_0 \cos\varphi \\
m_l &= -m \cdot m_0 \sin\varphi,
\end{aligned}
\tag{4}
$$

with $m = \pm 1$ giving the curling sense of the vortex and m_0 being the magnitude of the magnetization normalized by the saturation magnetization. This oversimplified model does not introduce any radial dependence, but is sufficient to capture the essence of MHD. Similarly, we write the incident field as a P-polarized twisted beam close to normal incidence, so that we can identify the coordinates in the transverse plane of the beam and the sample plane. The reflected field writes

$$
E_r(\ell, m) = \begin{pmatrix} r_{pp}(1 + r_0^t m \cdot m_0 \cos\varphi) & -r_{ps}^l m \cdot m_0 \sin\varphi \\ r_{ps}^l m \cdot m_0 \sin\varphi & r_{ss} \end{pmatrix} \cdot \begin{pmatrix} e^{i\ell\varphi} \\ 0 \end{pmatrix} = \begin{pmatrix} r_{pp}e^{i\ell\varphi} + r_{pp}r_0^t \frac{m \cdot m_0}{2}\left(e^{i(\ell+1)\varphi} + e^{i(\ell-1)\varphi}\right) \\ -ir_{ps}^l \frac{m \cdot m_0}{2}\left(e^{i(\ell+1)\varphi} - e^{i(\ell-1)\varphi}\right) \end{pmatrix}.
\tag{5}
$$

As apparent in the last term of Eq. 5, the P-component of the reflected field is a superposition of OAM states ℓ, $\ell-1$ and $\ell+1$ (the last two having the same weight), while the S-component only has equal contributions from the $\ell-1$ and $\ell+1$ modes. In the end, there is no net OAM transfer upon reflection on the MV: the average OAM of the reflected field is still ℓ. One can intuitively understand this feature by recalling that it is the transverse magnetization that acts on the phase of the beam. While travelling along a circle about the center of the MV, the transverse magnetization goes up and down sinusoidally, thus the local tilt imparted to the light wave-fronts is successively positive and negative, and the net OAM transfer is null.

3.2 Simulations

We now turn to a more complete and realistic model of the experiment, sketched in Fig. 1. We consider a P-polarized collimated gaussian light beam of wavelength λ, acquiring OAM $\ell = 1$ by going through a spiral phase mask, focused on a MV. Intensity and phase maps of the beam are shown in Fig. 1(a,d). The MV is modelled as a ferromagnetic dot, with the sign of its toroidal moment designed by $m = \pm 1$. Amplitude and direction of the magnetization are shown in Fig. 1(b,e) for $m = +1$. The MV is tilted by θ with respect to the z-axis of the incoming beam. Although the main conclusions are unchanged for large angles, we consider a small angle $\theta = 5°$ in order to avoid spurious anamorphisms.[32] We also assume the incoming beam perfectly centered on the MV. We consider wavelengths significantly larger than the typical size for the surface rugosity (below 1 nm). The beam waist at focus is much smaller than the MV diameter, avoiding the treatment of edge diffraction. With these constraints, a suitable wavelength range for MHD is $10\,\text{nm} \lesssim \lambda \lesssim 1000$ nm, which covers magnetization sensitive electron transitions in most elements of interest for magnetic materials.

We develop a numerical example using the magneto-optical constants of Fe at a wavelength of ≈ 23.5 nm (XUV range) corresponding to the $3p \rightarrow 3d$ electron excitation. Thus we build a model of the reflectivity coefficients yielding the maps displayed in Fig. 1(c),(f). We computed the following values for their maxima at $\theta = 5°$:[35] $r_{pp} = 0.027e^{-1.38j}$, $r_0^t = 0.038e^{-0.11j}$ and $r_{ps}^l = 0.00051e^{-1.49j}$. The two coefficients $(r_{pp} \cdot r_0^t)$ and r_{ps}^l have similar amplitude, respectively 3.8% and 1.9% of r_{pp}.
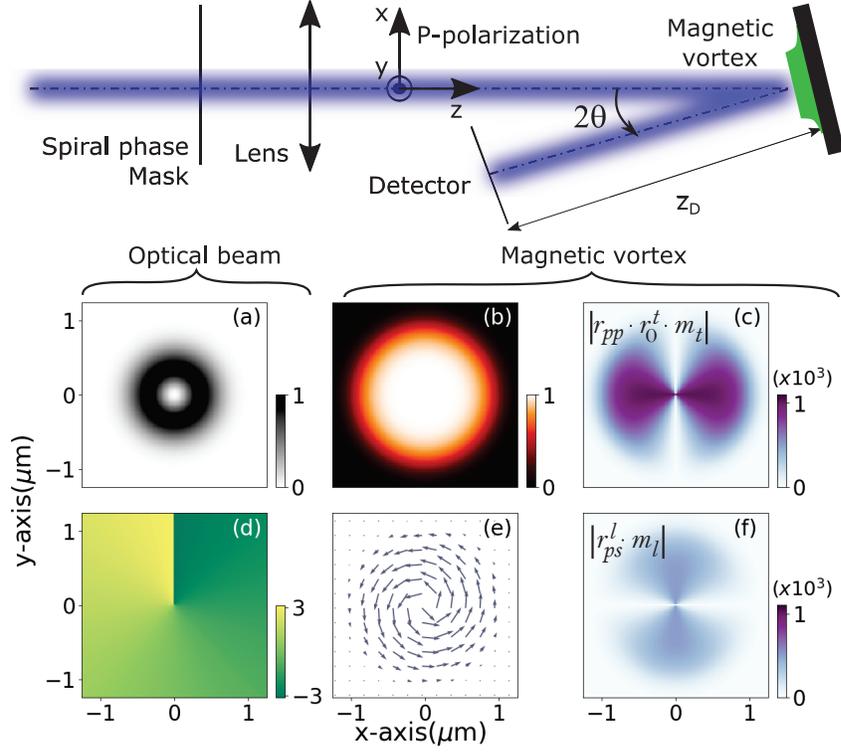
Figure 1. (top) Schematic layout of the conceptual experiment. (bottom) Intensity (a) and phase (d) maps of the incoming beam. Amplitude (b) and direction (e) of the magnetization vector of the MV for $m = +1$. (c,f) Maps of the amplitude of the MOKE coefficients $|r_{pp} \cdot r_0^t m_t|$ and $|r_{ps}^l m_l|$, respectively.
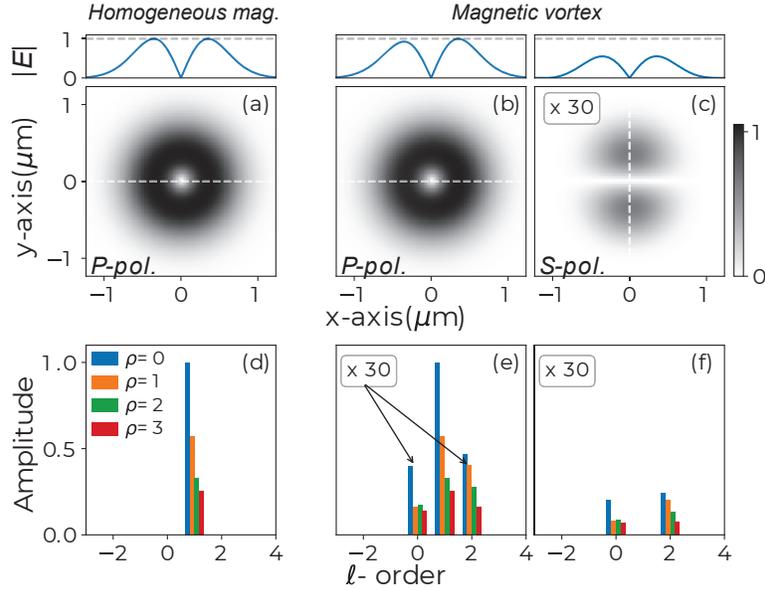

Figure 2. (a) Electric field amplitude after reflection of a P-polarized beam with OAM $\ell = 1$ by a magnetic dot with constant magnetization direction and (b,c) by a MV considering P and S outgoing polarizations respectively. The profile along the white dashed lines are shown in the top panels. (d-f) Magnitude of the coefficients of the decomposition on the LG basis (ℓ, ρ).

The analysis of the reflected beam in the near-field after reflection is presented in Fig. 2. We compare amplitude (a-c) and Laguerre-Gaussian (LG) modes decomposition (d-f) for two cases: a dot with a single domain of constant magnetization along the y axis and the MV sketched in Fig. 1, with projection on the P and S field components. In the first case the beam maintains its symmetry. On the contrary, the MV leads to an asymmetry in the intensity profile of the P-component, and the appearance of an S-component, as apparent in the line-outs displayed on top. As expected from the comparison of L-MOKE and T-MOKE, the S component of the reflected beam is only present where the local longitudinal magnetization is significant, but vanishes at locations where the magnetization is purely transverse.

To better characterize the asymmetry of the near-field beam, we decompose the computed field on an LG-basis with azimuthal and radial indices (ℓ, ρ). Due to the finite size of the MV and the imperfect transformation towards a LG mode by the optical setup, even for the single domain case [Fig. 2(d)] several radial ρ modes are populated, but no other azimuthal modes than $\ell = 1$. For the MV case we find instead that also the modes $\ell = 0, 2$ are populated [Fig. 2(e,f)], in agreement with the above prediction. It is worth noticing that these conclusions do not hold if the beam was not centered on the MV or for a significant incidence angle θ. However, for odd incoming values of ℓ, this latter spurious effect does not mix with the one described here.[32] Furthermore, we notice that the ratio of the weights of the newly populated azimuthal modes over the incoming one is of the same order as that of magnetic over non magnetic reflectivity constants: 2% for the S-component, 4% for the P-component.

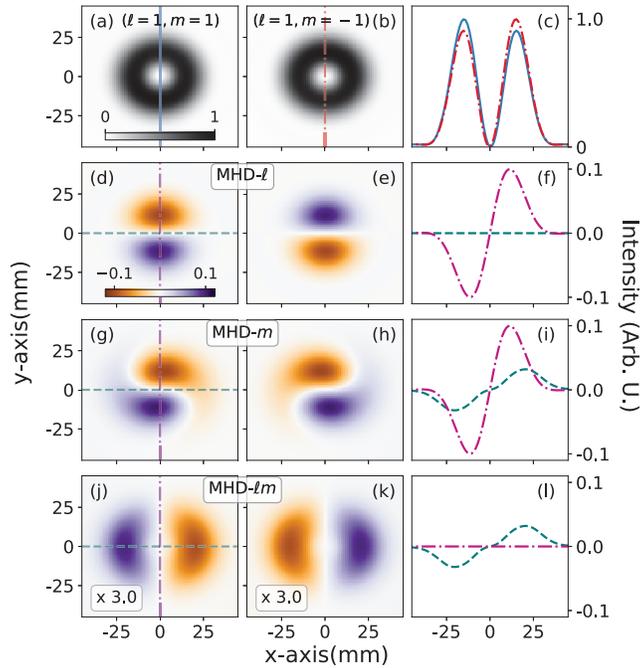## 4. MAGNETIC HELICOIDAL DICHROISM IN THE FAR FIELD

Figure 3. (a) Far-field intensity for $(\ell, m) = (1, 1)$ and (b) for $(\ell, m) = (1, -1)$, with the same color scale. (c) Profiles through the y axis for map (a) (blue straight) and (b) (red dotted). (d-e): MHD-ℓ, (g-h): MHD-m, (j-k): MHD-ℓm, and (f,i,l) corresponding lineouts.

Since LG modes are eigensolutions of the paraxial propagation equation, the intensity profile in the far field will show interferences of the modes $\ell = 0$ and $\ell \pm 1$, resulting in asymmetries. We compute the sum of the intensities of the P and S polarization components for the four different combinations of $(\ell, m) = (\pm 1, \pm 1)$. Two examples are shown in Fig. 3(a-b). In the considered configuration, MHD appears only in the P component,[32] therefore uncontrolled polarizing mirrors in the XUV transport line will not affect the dichroism. As for MCD, for which the dichroism can be observed by inverting either the magnetization or the photon SAM (i.e., the

circular polarization helicity), MHD can be observed by inverting either all the magnetization signs (MHD-m) or the sign of the photon OAM (MHD-ℓ). Contrary to MCD, though, the inversion of both does not lead to an identically zero MHD-ℓm signal. Denoting $I_{\ell,m}$ the far field intensity of the reflected beam, the three dichroisms are given by

$$\text{MHD-}\ell = I_{\ell,m} - I_{-\ell,m} \tag{6a}$$

$$\text{MHD-}m = I_{\ell,m} - I_{\ell,-m} \tag{6b}$$

$$\text{MHD-}\ell m = I_{\ell,m} - I_{-\ell,-m} . \tag{6c}$$

They are shown in Fig. 3, being non zero in all cases, with values up to 10%. Intuitively, this is related to the order of magnitude of the interference term between $\ell = 1$ and $\ell = 0$ modes: $\sqrt{|r_{pp}| \cdot |r_{pp} \cdot r_0^t|}/(|r_{pp}| + |r_{pp} \cdot r_0^t|) \simeq \sqrt{|r_0^t|} \simeq 20\%$. This interference term makes the dichroism detectable, even if away from the Brewster angle where magneto-optical differential signals are usually enhanced. The φ periodicity observed in Fig. 3 is a consequence of the mode content found in Fig. 2(e), where the $\Delta\ell = \pm 1$ modes interfere with the fundamental ℓ mode. The information carried by the three dichroic signals is actually redundant. Indeed, we have MHD-ℓ = MHD-ℓm + MHD-m [†].

It is possible to analytically derive the shape of the MHD images in the case of reflection off a MV, using the general expressions for MHD found in Ref.[32] We find

$$\text{MHD-}\ell \approx m|r_0^t| \cos\varphi_0^t \left(-\mathcal{H}_{-1} - \mathcal{H}_1\right) \sin\varphi \tag{7a}$$

$$\text{MHD-}m \approx m|r_0^t| \sum_{n=\pm 1} \mathcal{H}_n \sin(\varphi + n\varphi_0^t) \tag{7b}$$

$$\text{MHD-}\ell m \approx m|r_0^t| \sin\varphi_0^t \left(\mathcal{H}_{-1} - \mathcal{H}_1\right) \cos\varphi, \tag{7c}$$

where $\varphi_0^t = \arg(r_0^t)$ and the function $\mathcal{H}_n = \mathcal{H}_n(kr, z_D)$ [‡] depends on the beam wavevector k, radial parameter r and observation distance z_D. Interestingly, we observe that two MHD signals, MHD-ℓ and MHD-ℓm for example, allow to extract the complex magneto-optical constant r_0^t by fitting the intensity maps to $\sin\varphi$ and $\cos\varphi$ functions.[32]

5. CONCLUSION

We presented an analytical and numerical model for the reflection of a light beam carrying OAM by a magnetic vortex. Because of magneto-optic interaction, the incoming ℓ mode is redistributed into the $\ell \pm 1$ modes. Consequently, the far field intensity of the reflected beam is spatially asymmetric because of interference of different modes, and results in a dichroism signal when switching the OAM sign (MHD-ℓ), or the magnetic vortex curling direction (MHD-m). The two are qualitatively different, so also switching both leads to dichroism (MHD-ℓm). As an application, we showed how to use MHD in order to extract the value of a MOKE constant with high sensitivity without any polarization device in the experiment. Furthermore, thanks to the complete model presented in a recent work,[32] this approach can be easily extended to other targets, from antivortices to virtually any inhomogeneus magnetic structure, with the possibility to tailor the most suitable experimental conditions in terms of light polarization and reflection geometry. Conversely, different magnetic geometries could be fabricated, in order to characterize the OAM mode content of a light beam.

MHD is both an interesting platform for the basic study of light-matter interaction and a potentially rich spectroscopic tool. On one side, we have the coupling of a beam carrying topological charge with a magnetic material, with MV being a particularly interesting case given its topological nature as well. Also, we did not consider the microscopic, local differential response when the beam is reflected, and coupling with SAM[31] would

---

[†] This can be obtained as MHD-ℓ − MHD-ℓm = $-I_{-\ell,m} + I_{-\ell,-m} = -P_x(I_{\ell,m} - I_{\ell,-m})$ = MHD-m, where P_x is a parity inversion operator, acting on the x coordinate.

[‡] The $\mathcal{H}_n$ function is given by $\mathcal{H}_n(kr, z) = \frac{H_{n,\ell}(kr,z)}{H_{0,\ell}(kr,z)}$, with the function $H_{n,\ell}$ defined in Ref.[32] $n = \pm 1$ for the MV is the index of decomposition of the magnetic structure in the LG basis, ℓ is the OAM of the incoming beam, which we considered equal to ± 1 here.

certainly enrich the method. On the other side, since the XUV spectral range is accessible to high harmonic generation sources and to free electron lasers, a natural extension to the study of ultrafast dynamics in the femtosecond and attosecond regimes is conceivable. This would provide access to the dynamics of MV, which are known to respond to femtosecond pulses,[19] and potentially to manipulate them.

ACKNOWLEDGMENTS

REFERENCES

[1] Chen, T., Dumas, R. K., Eklund, A., Muduli, P. K., Houshang, A., Awad, A. A., Durrenfeld, P., Malm, B. G., Rusu, A., and Akerman, J., "Spin-Torque and Spin-Hall Nano-Oscillators," *Proceedings of the IEEE* **104**(10), 1919–1945 (2016).

[2] Dieny, B. and Chshiev, M., "Perpendicular magnetic anisotropy at transition metal/oxide interfaces and applications," *Reviews of Modern Physics* **89**(2) (2017).

[3] Yamada, K., Kasai, S., Nakatani, Y., Kobayashi, K., Kohno, H., Thiaville, A., and Ono, T., "Electrical switching of the vortex core in a magnetic disk," *Nature Materials* **6**(4), 270–273 (2007).

[4] Choi, H. S., Kang, S. Y., Cho, S. J., Oh, I.-Y., Shin, M., Park, H., Jang, C., Min, B.-C., Kim, S.-I., Park, S.-Y., and Park, C. S., "Spin nano-oscillator-based wireless communication," *Scientific Reports* **4** (jun 2014).

[5] Locatelli, N., Hamadeh, A., Araujo, F. A., Belanovsky, A. D., Skirdkov, P. N., Lebrun, R., Naletov, V. V., Zvezdin, K. A., Muñoz, M., Grollier, J., Klein, O., Cros, V., and de Loubens, G., "Efficient Synchronization of Dipolarly Coupled Vortex-Based Spin Transfer Nano-Oscillators," *Scientific Reports* **5** (nov 2015).

[6] Wei, J., Fang, B., Wu, W., Cao, K., Chen, H.-H., Zhang, Y., Zeng, Z., Wu, H., Bai, M., and Zhao, W., "Amplitude and frequency modulation based on memristor-controlled spin nano-oscillators," *Nanotechnology* **31**, 45202 (oct 2019).

[7] Torrejon, J., Riou, M., Araujo, F. A., Tsunegi, S., Khalsa, G., Querlioz, D., Bortolotti, P., Cros, V., Yakushiji, K., Fukushima, A., Kubota, H., Yuasa, S., Stiles, M. D., and Grollier, J., "Neuromorphic computing with nanoscale spintronic oscillators," *Nature* **547**, 428–431 (jul 2017).

[8] Romera, M., Talatchian, P., Tsunegi, S., Araujo, F. A., Cros, V., Bortolotti, P., Trastoy, J., Yakushiji, K., Fukushima, A., Kubota, H., Yuasa, S., Ernoult, M., Vodenicarevic, D., Hirtzlin, T., Locatelli, N., Querlioz, D., and Grollier, J., "Vowel recognition with four coupled spin-torque nano-oscillators," *Nature* **563**, 230–234 (oct 2018).

[9] Leulmi, S., Chauchet, X., Morcrette, M., Ortiz, G., Joisten, H., Sabon, P., Livache, T., Hou, Y., Carriére, M., Lequien, S., and Dieny, B., "Triggering the apoptosis of targeted human renal cancer cells by the vibration of anisotropic magnetic particles attached to the cell membrane," *Nanoscale* **7**(38), 15904–15914 (2015).

[10] Peixoto, L., Magalhães, R., Navas, D., Moraes, S., Redondo, C., Morales, R., Araújo, J. P., and Sousa, C. T., "Magnetic nanostructures for emerging biomedical applications," *Applied Physics Reviews* **7**, 11310 (mar 2020).

[11] Zhang, X., Zhou, Y., Song, K. M., Park, T.-E., Xia, J., Ezawa, M., Liu, X., Zhao, W., Zhao, G., and Woo, S., "Skyrmion-electronics: writing, deleting, reading and processing magnetic skyrmions toward spintronic applications," *Journal of Physics: Condensed Matter* **32**, 143001 (jan 2020).

[12] Fernández-Pacheco, A., Streubel, R., Fruchart, O., Hertel, R., Fischer, P., and Cowburn, R. P., "Three-dimensional nanomagnetism," *Nature Communications* **8** (jun 2017).

[13] Shinjo, T., "Magnetic Vortex Core Observation in Circular Dots of Permalloy," *Science* **289**, 930–932 (aug 2000).

[14] Bader, S. D., "Colloquium: Opportunities in nanomagnetism," *Reviews of Modern Physics* **78**, 1–15 (jan 2006).

[15] Hlinka, J., "Eight Types of Symmetrically Distinct Vectorlike Physical Quantities," **113**, 165502 (Oct. 2014).

[16] Braun, H.-B., "Topological effects in nanomagnetism: from superparamagnetism to chiral quantum solitons," *Advances in Physics* **61**(1), 1–116 (2012).

[17] Choe, S.-B., "Vortex Core-Driven Magnetization Dynamics," *Science* **304**, 420–422 (apr 2004).

[18] Guslienko, K. Y., Han, X. F., Keavney, D. J., Divan, R., and Bader, S. D., "Magnetic Vortex Core Dynamics in Cylindrical Ferromagnetic Dots," *Phys. Rev. Lett.* **96**, 67205 (feb 2006).

[19] Fu, X., Pollard, S. D., Chen, B., Yoo, B.-K., Yang, H., and Zhu, Y., "Optical manipulation of magnetic vortices visualized in situ by Lorentz electron microscopy," *Science Advances* **4**(7) (2018).

[20] Schneider, M., Hoffmann, H., and Zweck, J., "Lorentz microscopy of circular ferromagnetic permalloy nanodisks," *Applied Physics Letters* **77**(18), 2909–2911 (2000).

[21] Wachowiak, A., "Direct Observation of Internal Spin Structure of Magnetic Vortex Cores," *Science* **298**, 577–580 (oct 2002).

[22] van Houselt, A. and Zandvliet, H. J. W., "Colloquium: Time-resolved scanning tunneling microscopy," *Reviews of Modern Physics* **82**, 1593–1605 (may 2010).

[23] Tian, Y., Yang, F., Guo, C., and Jiang, Y., "Recent Advances in Ultrafast Time-Resolved Scanning Tunneling Microscopy," *Surface Review and Letters* **25**, 1841003 (jan 2018).

[24] Beaurepaire, E., Merle, J.-C., Daunois, A., and Bigot, J.-Y., "Ultrafast Spin Dynamics in Ferromagnetic Nickel," *Phys. Rev. Lett.* **76**, 4250–4253 (may 1996).

[25] Kirilyuk, A., Kimel, A. V., and Rasing, T., "Ultrafast optical manipulation of magnetic order," *Reviews of Modern Physics* **82**, 2731–2784 (sep 2010).

[26] Siegrist, F., Gessner, J. A., Ossiander, M., Denker, C., Chang, Y.-P., Schröder, M. C., Guggenmos, A., Cui, Y., Walowski, J., Martens, U., Dewhurst, J. K., Kleineberg, U., Münzenberg, M., Sharma, S., and Schultze, M., "Light-wave dynamic control of magnetism," *Nature* **571**, 240–244 (jun 2019).

[27] Vansteenkiste, A., Chou, K. W., Weigand, M., Curcic, M., Sackmann, V., Stoll, H., Tyliszczak, T., Woltersdorf, G., Back, C. H., Schütz, G., and Waeyenberge, B. V., "X-ray imaging of the dynamic magnetic vortex core deformation," *Nature Physics* **5**, 332–334 (mar 2009).

[28] Chauleau, J.-Y., Legrand, W., Reyren, N., Maccariello, D., Collin, S., Popescu, H., Bouzehouane, K., Cros, V., Jaouen, N., and Fert, A., "Chirality in Magnetic Multilayers Probed by the Symmetry and the Amplitude of Dichroism in X-Ray Resonant Magnetic Scattering," *Physical Review Letters* **120**, 37202 (jan 2018).

[29] Spezzani, C., Ferrari, E., Allaria, E., Vidal, F., Ciavardini, A., Delaunay, R., Capotondi, F., Pedersoli, E., Coreno, M., Svetina, C., Raimondi, L., Zangrando, M., Ivanov, R., Nikolov, I., Demidovich, A., Danailov, M. B., Popescu, H., Eddrief, M., De Ninno, G., Kiskinova, M., and Sacchi, M., "Magnetization and Microstructure Dynamics in Fe/MnAs/GaAs(001): Fe Magnetization Reversal by a Femtosecond Laser Pulse," *Phys. Rev. Lett.* **113**, 247202 (dec 2014).

[30] van Veenendaal, M., "Interaction between x-ray and magnetic vortices," *Physical Review B* **92** (dec 2015).

[31] Kfir, O., Zayko, S., Nolte, C., Sivis, M., Möller, M., Hebler, B., Arekapudi, S. S. P. K., Steil, D., Schäfer, S., Albrecht, M., Cohen, O., Mathias, S., and Ropers, C., "Nanoscale magnetic imaging using circularly polarized high-harmonic radiation," *Science Advances* **3**, eaao4641 (dec 2017).

[32] Fanciulli, M., Bresteau, D., Vimal, M., Luttmann, M., Sacchi, M., and Ruchon, T., "Electromagnetic theory of helicoidal dichroism in reflection from magnetic structures," *Phys. Rev. A* **103**, 013501 (Jan 2021).

[33] Fanciulli, M., Pancaldi, M., Pedersoli, E., Vimal, M., Bresteau, D., Luttmann, M., De Angelis, D., Ribič, P. c. v. R., Rösner, B., David, C., Spezzani, C., Manfredda, M., Sousa, R., Prejbeanu, I.-L., Vila, L., Dieny, B., De Ninno, G., Capotondi, F., Sacchi, M., and Ruchon, T., "Observation of magnetic helicoidal dichroism with extreme ultraviolet light vortices," *Phys. Rev. Lett.* **128**, 077401 (Feb 2022).

[34] Piovera, C., "Ultrafast laser induced dynamics in ferromagnets: towards the control of the spin order from the femtosecond to the sub-nanosecond time scale," (2013).

[35] Valencia, S., Gaupp, A., Gudat, W., Mertins, H.-C., Oppeneer, P. M., Abramsohn, D., and Schneider, C. M., "Faraday rotation spectra at shallow core levels: 3p edges of Fe, Co, and Ni," *New Journal of Physics* **8**, 254 (oct 2006).